



ARTICLE

<https://doi.org/10.1038/s41467-019-10405-8>

OPEN

Theory of the field-revealed Kitaev spin liquid

Jacob S. Gordon ¹, Andrei Catuneanu¹, Erik S. Sørensen ² & Hae-Young Kee^{1,3}

Elementary excitations in entangled states such as quantum spin liquids may exhibit exotic statistics different from those obeyed by fundamental bosons and fermions. Non-Abelian anyons exist in a Kitaev spin liquid—the ground state of an exactly solvable model. A smoking-gun signature of these excitations, namely a half-integer quantized thermal Hall conductivity, was recently reported in α -RuCl₃. While fascinating, a microscopic theory for this phenomenon remains elusive because the pure Kitaev model cannot display this effect in an intermediate magnetic field. Here we present a microscopic theory of the Kitaev spin liquid emerging between the low- and high-field states. Essential to this result is an anti-ferromagnetic off-diagonal symmetric interaction which allows the Kitaev spin liquid to protrude from the ferromagnetic Kitaev limit under a magnetic field. This generic model displays a strong field anisotropy, and we predict a wide spin liquid regime when the field is perpendicular to the honeycomb plane.

¹Department of Physics, University of Toronto, Toronto, ON M5S 1A7, Canada. ²Department of Physics and Astronomy, McMaster University, Hamilton, ON L8S 4M1, Canada. ³Canadian Institute for Advanced Research, CIFAR Program in Quantum Materials, Toronto, ON M5G 1M1, Canada. Correspondence and requests for materials should be addressed to H.-Y.K. (email: hykee@physics.utoronto.ca)

The Kitaev spin liquid (KSL) is a long-range entangled state on a honeycomb lattice¹, which hosts non-Abelian^{1–3} anyon excitations in a magnetic field. It has been proposed that topological quantum computation can be performed via braiding of non-Abelian anyons⁴, meaning the KSL is of both practical, and fundamental interest. However, it has been challenging to find a solid state realization of Kitaev physics, which has been the focus of recent research. Several honeycomb materials have been suggested as KSL candidates, namely Mott insulators with strong spin-orbit coupling (SOC) featuring 4d or 5d transition metal elements^{5–9}. Proposals so far include the iridates $A_2\text{IrO}_3$ ^{5,6,10–13} ($A=\text{Li, Na}$), and $\alpha\text{-RuCl}_3$ ^{14–18}. However, all these candidates exhibit magnetic ordering at low temperatures^{17,19–26} which masks potential Kitaev physics. Later theoretical^{27–29} and experimental^{30–33} results suggest that $\alpha\text{-RuCl}_3$ may enter a field-induced spin liquid, but there has been no evidence that it is a chiral spin liquid until a half-integer quantized thermal Hall conductivity was reported in $\alpha\text{-RuCl}_3$ ³⁴; a strong indication^{35–37} of chiral edge currents of Majorana fermions (MFs) predicted in a KSL.

While the observation of a half-integer quantized thermal Hall conductivity is the first experimental evidence of charge-neutral non-Abelian anyons in spin systems, a microscopic theory describing their appearance under a field in $\alpha\text{-RuCl}_3$ is missing. This is because, if the dominant interaction in $\alpha\text{-RuCl}_3$ is the ferromagnetic (FM) Kitaev term (as shown through ab-initio studies^{25,26} and spin wave analysis³⁶), the FM Kitaev phase is almost immediately destroyed, and the polarized state appears in an applied field^{38–40} with no intervening phase. This can be contrasted with the antiferromagnetic (AFM) Kitaev model which hosts a potentially gapless spin liquid under a field, supported by several numerical studies^{39–47}. However, this intermediate gapless spin liquid cannot explain the half-integer thermal Hall effect observed in $\alpha\text{-RuCl}_3$. Thus, searching for a chiral spin liquid offering a half-integer thermal Hall effect in an intermediate magnetic field remains a challenging task.

Here we present a microscopic theory in which the KSL is revealed under a magnetic field. The key to our result is an AFM symmetric off-diagonal Γ interaction, which is essential to stabilize the otherwise fragile KSL under intermediate fields. The intermediate phase emerges between the low-field and high-field phases as Γ increases, and is adiabatically connected to the pure FM Kitaev phase at zero field, providing evidence that it is the KSL. We introduce a microscopic theory with a brief review of the generic nearest neighbor spin model for spin-orbit coupled honeycomb materials, appropriate for $\alpha\text{-RuCl}_3$.

Results

Model. The nearest neighbor model has been derived in refs. 5,12,13 based on a strong coupling expansion of the Kanamori Hamiltonian. The combination of crystal field splitting and strong spin-orbit coupling leads to a model based on pseudospin- $\frac{1}{2}$ local moments with bond-dependent interactions. On a bond of type $\gamma \in \{x, y, z\}$ with sites j, k , the nearest-neighbor spin Hamiltonian is taken to be of the $J\text{-}K\text{-}\Gamma$ form¹³

$$\mathcal{H}_{jk}^\gamma = JS_j \cdot S_k + KS_j^\alpha S_k^\alpha + \Gamma \left(S_j^\alpha S_k^\beta + S_j^\beta S_k^\alpha \right) + \Gamma' \left(S_j^\alpha S_k^\gamma + S_j^\gamma S_k^\alpha + S_j^\beta S_k^\gamma + S_j^\gamma S_k^\beta \right), \quad (1)$$

where α, β are the remaining spin components in $\{x, y, z\}/\{\gamma\}$. The spin components are directed along the cubic axes of the underlying ligand octahedra, so the honeycomb layer lies in a plane perpendicular to the [111] spin direction as shown in Fig. 1a. A small Γ' is present due to trigonal distortion of ligand octahedra in the real material. Here we omit the Heisenberg J for

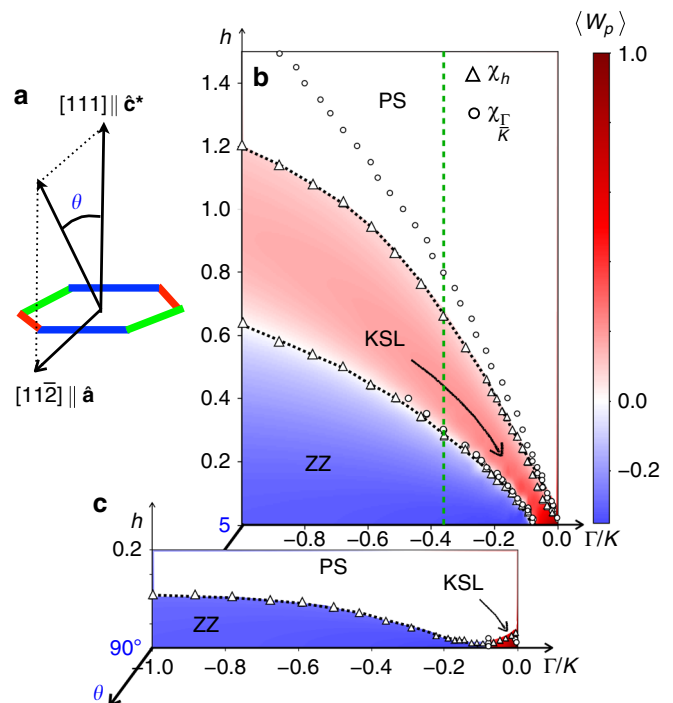


Fig. 1 ED phase diagrams. **a** The angle θ is measured from [111] towards the in-plane $[11\bar{2}]$ direction. Phase diagrams in the $\Gamma/K - h$ plane (FM Kitaev and AFM Γ) obtained using ED on the 24-site honeycomb cluster are shown for **b** $\theta = 5^\circ$ and **c** $\theta = 90^\circ$ at a fixed $\Gamma' = -0.03$ in units of $\sqrt{K^2 + \Gamma^2} \equiv 1$. Circular and triangular markers represent peaks in the susceptibilities $\chi_{\Gamma/K}$ and χ_h , respectively. The intermediate-field KSL is adiabatically connected to the pure K limit at $h = 0$, as indicated by a black arrow inside the KSL. Colors represent the expectation value of the plaquette operator $\langle W_p \rangle$ in the ZZ and KSL, but not in the PS for clarity, which is discussed further in the main text. A sequence of phase transitions from ZZ order to the KSL, and finally the PS is found for $\theta = 5^\circ$, except near the pure K limit. The green line in **b** at $\Gamma/K \simeq -0.37$ denotes a representative slice where χ_h and $S(\mathbf{q})$ are plotted in Fig. 2

simplicity, and its effects are discussed later. Earlier studies^{14,26,29,48,49} noted that the Γ interaction with AFM sign may play an important role near the FM Kitaev regime to stabilize the spin liquid⁴⁸. Since $\alpha\text{-RuCl}_3$ has a dominant FM Kitaev interaction with AFM Γ , we focus on $\Gamma/K \in [-1, 0]$ with $\Gamma > 0$ and $K < 0$. The remaining parameters of the Hamiltonian are expressed in units of $\sqrt{K^2 + \Gamma^2} \equiv 1$.

To describe the effect of a magnetic field we consider a Zeeman term with isotropic g -factor

$$\mathcal{H}_Z = -h \sum_j \hat{\mathbf{h}} \cdot \mathbf{S}_j, \quad (2)$$

where h is the magnetic field strength, and $\hat{\mathbf{h}}$ is a unit vector specifying the field direction. The effect of an anisotropic g -factor is discussed later. In order to make a connection with the thermal Hall measurements³⁴ we focus on field directions in the $\hat{\mathbf{a}}\hat{\mathbf{c}}^*$ plane spanned by $[11\bar{2}]$ and $[111]$. The direction of the field in this plane is parameterized by an angle θ from the $[111]$ direction, as shown in Fig. 1a.

Exact diagonalization. Our main results are shown in Fig. 1b, c. Phase diagrams in the $\Gamma/K - h$ plane are shown for tilting angles (b) $\theta = 5^\circ$ and (c) 90° obtained through numerical exact diagonalization (ED) with fixed $\Gamma' = -0.03$ and $J = 0$. Details of the 24-site honeycomb cluster used are discussed in Supplementary

Note 1. Peaks in the susceptibilities $\chi_{\Gamma/K} = -\partial_{\Gamma/K}^2 e_0$ and $\chi_h = -\partial_h^2 e_0$, where $e_0 = E_0/N$ is the ground state energy density, are depicted as circles and triangles, respectively. There are three phases in the phase space, namely, zigzag (ZZ) magnetic order at low fields, the KSL, and a polarized state (PS) at high fields. Remarkably, we find an intermediate KSL sitting between ZZ order and the PS which is adiabatically connected to the pure K limit at $h = 0$.

The intermediate KSL begins from the pure FM K regime, i.e., bottom right corner of the phase diagram, which is unstable to a small magnetic field. However, it is stabilized by the AFM Γ term and extends above the ZZ phase in a magnetic field. For moderate Γ/K appropriate for α -RuCl₃—for example, $\Gamma/K \simeq -0.37$ indicated by the green dashed line in Fig. 1b—we observe two phase transitions from ZZ order to the KSL, and then from KSL to the PS as the field increases. Close to the Kitaev limit, the peak positions of the magnetic (χ_h) and Γ/K ($\chi_{\Gamma/K}$) susceptibilities agree well along the phase boundaries between the KSL and PS for each direction. At larger $\Gamma/|K|$ the singular points determining the phase boundaries start to deviate for $\theta = 5^\circ$, as seen through differing positions of circular and triangular markers in Fig. 1b. However, the anomalous peaks in $\chi_{\Gamma/K}$ in this region shrink significantly while the peaks in χ_h retain their sharpness. Since these peaks are not seen in χ_h , and there are strong variations within the PS in the quantities discussed below, we determine the KSL-PS phase boundary based on peaks in χ_h and attribute peaks in $\chi_{\Gamma/K}$ to large fluctuations above the KSL.

Interestingly, with a constant Γ' both the ZZ and KSL phases widen with increasing Γ as suggested by the curvature of the transition line in Fig. 1b. This behavior survives for further tilting of the magnetic field away from [111] with increased [112] in-plane component. However, the window of the KSL rapidly diminishes with tilting angle until a direct transition between ZZ order and the PS appears at large $\Gamma/|K|$, as shown in Fig. 1c for a [112] field. The critical field required to destroy the ZZ ordering drops dramatically with increasing θ . With an estimate of the energy unit as $\sqrt{K^2 + \Gamma^2} \sim 7$ meV, $h = 0.1$ corresponds to a field of ~ 10 T. This is within the range of fields required to kill the ZZ order in α -RuCl₃³⁴.

Since the pure Kitaev limit at $h = 0$ involves the fractionalization of spins into itinerant MFs and \mathbb{Z}_2 fluxes, another quantity that characterizes the KSL is the plaquette operator W_p ¹

$$W_p = 2^6 S_1^x S_2^y S_3^z S_4^x S_5^y S_6^z, \quad (3)$$

defined on sites belonging to a hexagonal plaquette p . The pure KSL with $h = \Gamma = \Gamma' = 0$ (bottom right corner of the phase diagram) is a flux-free state with $W_p = +1$ on all plaquettes. A finite Γ , Γ' or h spoils the exact solubility of the Kitaev model, as they generate interactions among the MFs and \mathbb{Z}_2 fluxes. Despite the fact that plaquette operators are no longer conserved quantities $\langle W_p \rangle$ remains positive in the KSL, denoted by red colors in Fig. 1. At the same time the plaquette expectation value is negative in the ZZ ordered phase, as denoted by blue colors in Fig. 1, distinguishing it from the neighboring KSL. Due to this sign difference, the phase boundary between KSL and ZZ is accompanied by a vanishing $\langle W_p \rangle$ and seen through the rapid color change in Fig. 1. This is a generic feature which also appears for an in-plane field of $\theta = 90^\circ$. Further details of the negative plaquette expectation in the ZZ phase can be found in Supplementary Note 3.

To confirm the ZZ magnetically ordered phase at low field, and the sequence of phase transitions, we compute the spin structure factor $S(\mathbf{q})$ for increasing values of h along the green dashed line of Fig. 1b where $\Gamma/K \simeq -0.37$. For low fields of $h < h_{c1}$, where h_{c1} is the position of the first transition, $S(\mathbf{q})$ displays sharp features

at the \mathbf{M} -point of the Brillouin zone (BZ) consistent with ZZ magnetic order as shown in Fig. 2a. Within the intermediate phase, $h_{c1} < h < h_{c2}$ where h_{c2} is the position of the second transition, $S(\mathbf{q})$ is diffuse with a soft peak at the Γ -point. Interestingly, an increased intensity at the Γ -point was observed in α -RuCl₃ under fields in a recent neutron scattering measurement⁵⁰. As expected, the PS exhibits a sharp feature at the Γ -point for $h > h_{c2}$. Note that the magnetization $m = -\partial_h e_0$ eventually saturates at $\frac{1}{2}$ in the PS at a field larger than h_{c2} , as shown in Fig. 2b indicating large spin fluctuations inside the PS.

Competition between ZZ and KSL. ZZ ordering at low fields can be traced back to the presence of other small interactions, such as such as a FM Γ' ^{5,12,13,27} and/or FM (J) and AFM third-nearest neighbor (J_3) Heisenberg interactions⁵¹. We have considered Γ' as a minimal nearest-neighbor perturbation away from the $K - \Gamma$ model which induces ZZ order at low fields. The combination of $J < 0$ and $J_3 > 0$ has a similar effect to Γ' in that their combination can also induce ZZ ordering^{13,51}. Inclusion of these small terms would not alter our main results as they further stabilize the ZZ phase. However, the combined strength of terms stabilizing the ZZ order should be small enough to maintain the intermediate KSL.

The particular values of Γ' used in our calculations were chosen based on the following criteria. For $\Gamma' = 0$ the phase to the left of the KSL at larger $\Gamma/|K|$ is non-magnetic, as discussed in the Underlying Phase Diagram section, and develops ZZ magnetic order as $\Gamma' < 0$ is introduced. The magnitude $|\Gamma'|$ was chosen to be the smallest value such that ZZ magnetic order develops within this phase. If $|\Gamma'|$ becomes too large then the KSL at $h = 0$ will be wiped out entirely. To quantify this, we have calculated $\chi_{\Gamma/K}$ with ED on a 24-site honeycomb cluster near the Kitaev limit at $h = 0$ for different values of Γ' . As $|\Gamma'|$ increases, the ZZ ordered phase expands while the KSL shrinks at $h = 0$ as shown in Fig. 3a. The

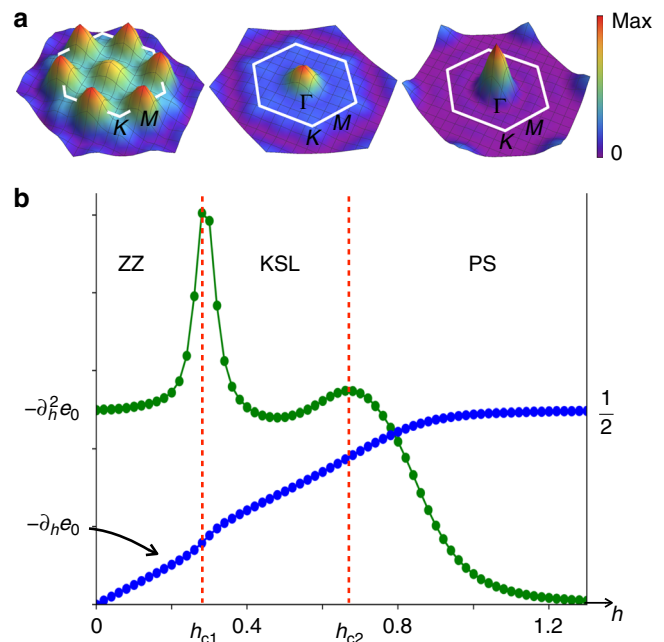


Fig. 2 Sequence of phases in a magnetic field. **a** Spin structure factor $S(\mathbf{q})$ within the ZZ, KSL, and PS phases. **b** $\chi_h = -\partial_h^2 e_0$ and magnetization $m = -\partial_h e_0$ as a function of a 5° tilted field are shown for a fixed $\Gamma/K \simeq -0.37$, indicated by a green dashed line in Fig. 1b. The field strengths h_{c1} and h_{c2} are the critical values at which the transitions from the ZZ to KSL, and the KSL to PS occur, respectively

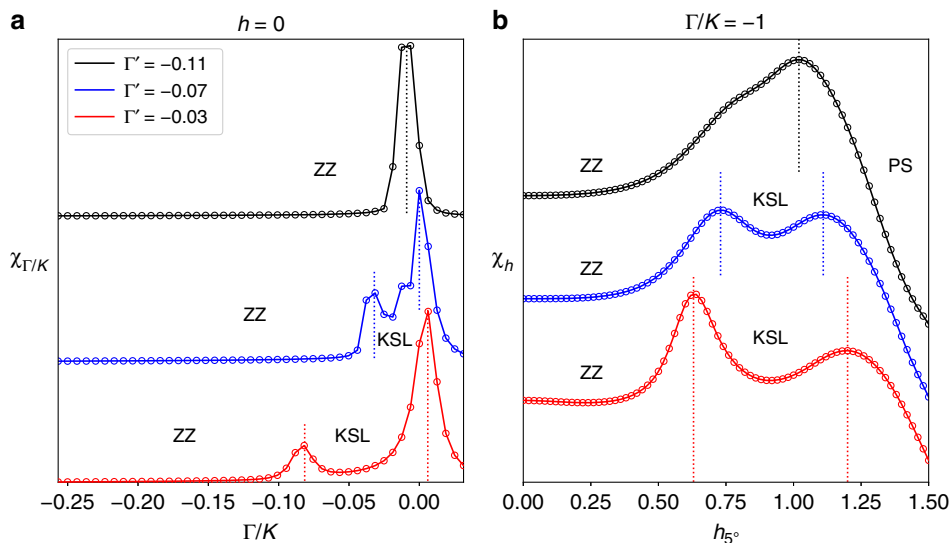


Fig. 3 Effect of Γ' on the intermediate phase. The role of Γ' is illustrated through cuts of the susceptibilities for increasing values of $|\Gamma'|$ as calculated with ED on a 24-site honeycomb cluster. **a** The susceptibility $\chi_{\Gamma/K}$ is shown at $h=0$ near the Kitaev limit for $\Gamma' = -0.03, -0.07,$ and -0.11 . Peak values of $\chi_{\Gamma/K}$ are scaled to the same number and are offset for visibility. With increasing $|\Gamma'|$ the ZZ phase is seen to expand as the KSL shrinks, and the KSL disappears entirely beyond $\Gamma'_c \simeq -0.1$. **b** The magnetic susceptibility χ_h is shown for a 5° tilted field at $\Gamma/K = -1$ where the intermediate phase is largest for $\Gamma' = -0.03$. Values of χ_h are not scaled, but simply offset for visibility. A similar trend is found where the size of the intermediate phase shrinks with increasing $|\Gamma'|$. The intermediate KSL disappears beyond $\Gamma'_c \simeq -0.1$ where the KSL at $h=0$ is overtaken by ZZ magnetic order. Vertical dashed lines represent the position of phase transitions

KSL at $h=0$ is found to disappear entirely beyond $\Gamma'_c \simeq -0.1$. Evolution of the intermediate-field KSL with Γ' is seen in Fig. 3b through the magnetic susceptibility χ_h in a 5° field at $\Gamma/K = -1$, where the intermediate phase is largest with $\Gamma' = -0.03$. Emergence of the intermediate-field KSL depends crucially on the survival of the pure Kitaev phase at $h=0$, because χ_h shows a single transition from ZZ to PS beyond $\Gamma'_c \simeq -0.1$. Quantifying the strengths of Γ', J, J_3 required for an intermediate KSL is left for a detailed future study.

DMRG. In order to check the dependence of this result on cluster geometry, we have also studied a two-leg honeycomb strip using density-matrix renormalization group (DMRG). We denote the total number of sites in the strip by N . This geometry has recently been used to study the Kitaev-Heisenberg model⁵², where it was found that its phase diagram displays a striking similarity with that of the 2D honeycomb lattice. For the $K - \Gamma$ model we find quantitative differences in the positions of the phase boundaries due to the cluster connectivity, but the main result of an emerging intermediate-field KSL remains the same. Further rationale for this choice of geometry is discussed in Supplementary Note 1.

Phase diagrams in the $\Gamma/K - h$ plane with $N=200$ and open boundary conditions (OBC) for tilting angles $\theta = 0^\circ, 5^\circ, 10^\circ,$ and 90° with fixed $\Gamma' = -0.1$ and $J = 0$ are shown in Fig. 4. The phase boundaries in Fig. 4, determined by peaks in χ_h or $\chi_{\Gamma/K}$, are represented by red lines. We find a qualitative similarity with the ED phase diagram of Fig. 1, showing a region of KSL which extends above the ZZ ordered phase and below the PS under a magnetic field. The KSL phase space shrinks rapidly as the in-plane component of the field becomes larger. As found with ED on the 24-site honeycomb cluster, the intermediate KSL at large $\Gamma/|K|$ disappears as the field tilts towards $\theta = 90^\circ$, leaving a single direct transition from ZZ to the PS. Crucially, a small region of KSL remains intact at smaller $\Gamma/|K|$. Thus, with the in-plane $[11\bar{2}]$ field the KSL is confined to a narrow range of low fields near the pure FM Kitaev limit. The same qualitative behavior is seen for another in-plane field direction of $[\bar{1}10]$ only for the 24-site

honeycomb cluster used with ED. On the two-leg honeycomb strip the KSL (in the region $\Gamma/|K| < \Gamma/|K|_c$ where $\Gamma/|K|_c$ is the transition point between ZZ and KSL at $h=0$) is immediately destroyed by any non-zero field in this direction, as shown in Supplementary Fig. 3. While this is consistent with the observation that there is no \mathbb{Z}_2 topological order when a certain mirror symmetry is preserved⁴⁶, the phase boundary is an artifact of the strip geometry.

The first row in Fig. 4 shows $\langle S_j^x S_k^x \rangle$ at separation $k - j = 50$ along the leg of the strip with maximum correlations as a function of field and Γ/K for different tilting angles of the field in the $\hat{a}\hat{c}^*$ plane. As expected, correlations are appreciable within the magnetically ordered and polarized states. The KSL phase is clearly distinguished from the surrounding ordered states by nearly vanishing $\langle S^x S^x \rangle$ ($= \langle S^y S^y \rangle$) spin correlations. However, spin-spin correlations need not be identically zero except at $h=0$ due to a component of the spin aligning with the field, which is more pronounced when h is large. The PS away from the pure Kitaev region shows large spin fluctuations, which is similar to the 24-site ED result where saturation of the magnetization occurs at higher fields above h_{c2} , and small peaks in $\chi_{\Gamma/K}$ only appear above the KSL-PS phase boundary.

In the bottom row of Fig. 4 we show plaquette-plaquette correlations $\langle W_p W_{p'} \rangle$ at separation $p' - p = 30$. Close to the Kitaev limit these correlations are nearly unity, consistent with $\langle W_p \rangle = +1$ in the K limit, and decrease with increasing field and $\Gamma/|K|$ within the KSL. This is expected because the magnetic field, as well as Γ, Γ' , introduces interactions among the MF and flux degrees of freedom. Interestingly, the plaquette-plaquette correlations, which approach $\langle W_p \rangle^2$ in the KSL at large separations, show large fluctuations in the PS above the KSL phase for 5° and 10° tilting angles. We note that these fluctuations in the PS for $\theta = 5^\circ$ and 10° disappear above the transition line between the KSL and PS determined by $\theta = 0^\circ$.

A representative cut of the phase diagram is presented in Fig. 5c, d as a function of a 5° tilted field with $\Gamma/K = -0.325$,

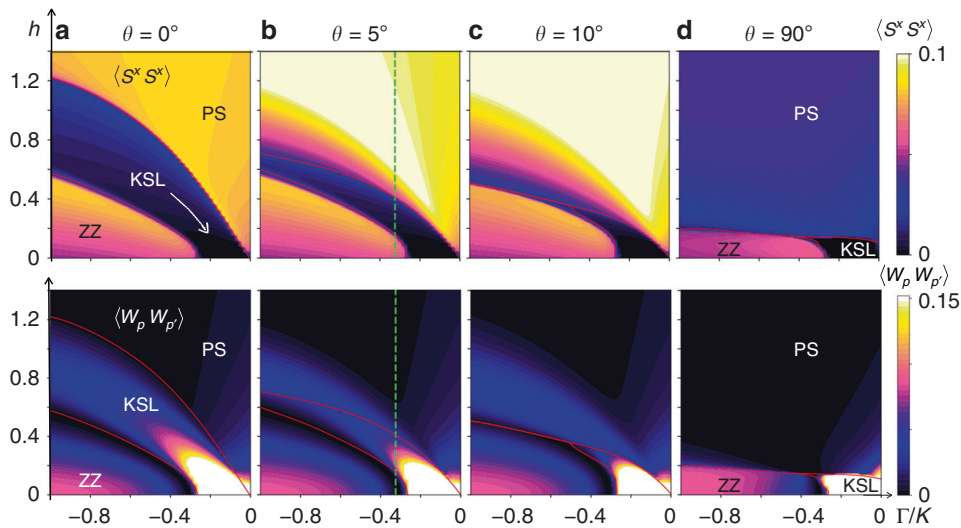


Fig. 4 DMRG phase diagrams. The spin-spin correlator $\langle S^x_i S^x_k \rangle$ at $k - j = 50$ along the leg of the strip with maximal correlations is shown in the first row, and the plaquette-plaquette correlator $\langle W_p W_{p'} \rangle$ at $p' - p = 30$ in the second as a function of Γ/K and h with $\Gamma' = -0.1$. These are obtained in the two-leg honeycomb strip using DMRG with $N = 200$ and OBC. The field directions are constant in a given column, which are **a** $\theta = 0^\circ$, **b** $\theta = 5^\circ$, **c** $\theta = 10^\circ$, and **d** $\theta = 90^\circ$ ($[1\bar{1}2]$ in-plane). Smooth curves fitted to peaks in either χ_h or $\chi_{\Gamma/K}$ are drawn with red lines. The white arrow in the spin-spin correlators of **a** indicates the smooth connection from the intermediate phase to the pure Kitaev limit. The dashed green line at $\Gamma/K = -0.325$ indicates a representative slice where certain quantities are plotted in Fig. 5 for a $\theta = 5^\circ$ tilted field

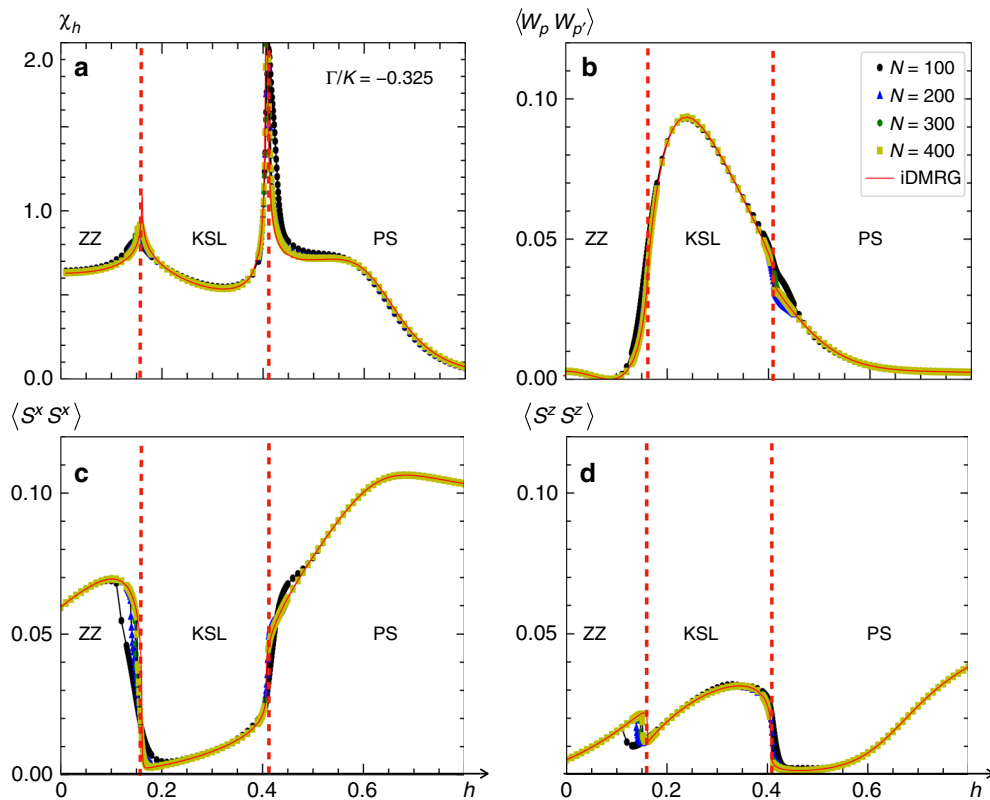


Fig. 5 Evolving correlations in a magnetic field. With $\Gamma/K = -0.325$ and $\Gamma' = -0.1$, quantities computed in the two-leg honeycomb strip with DMRG are plotted as a function of a 5° field for system sizes $N = 100, 200, 300, 400$ and infinite DMRG (iDMRG) as solid red line. **a** χ_h displays two peaks which sharpen with increasing system size. These transitions separate ZZ magnetic order and the PS from the intervening KSL. **b** Plaquette-plaquette correlations $\langle W_p W_{p'} \rangle$ are small within the ZZ and polarized phases, and become appreciable within the KSL. **c** Conversely, the xx spin-spin correlations $\langle S^x S^x \rangle$ are small within the KSL and large in the magnetically ordered phases. **d** Sharp changes in the zz spin-spin correlations are seen across the phase boundaries, and display a finite value consistent with a KSL in field. Spin and plaquette correlations are evaluated at the largest separation accessible in each cluster

which corresponds to the green line in Fig. 4b. With increasing field, a sequence of transitions from ZZ order to the KSL and finally the PS are evidenced by strong singular behavior in χ_h in Fig. 5a. The transition between ZZ order and the KSL is accompanied by a sharp increase in plaquette–plaquette correlations shown in Fig. 5b, and a larger value of $\langle W_p \rangle$ accordingly. Note that the maximum value of $\langle W_p W_{p'} \rangle \simeq 0.1$ corresponds to $\langle W_p \rangle \simeq 0.32$, as $\langle W_p W_{p'} \rangle$ approaches $\langle W_p \rangle^2$ at large distances. Components $\langle S^x S^x \rangle$ and $\langle S^z S^z \rangle$ of the spin–spin correlators are plotted in Fig. 5c, d. While the $\langle S^x S^x \rangle$ correlations are small in the KSL, the $\langle S^z S^z \rangle$ correlations are slightly larger. This is similar to the honeycomb cluster with ED, where a finite magnetization m is present in the KSL phase, as shown in Fig. 2b. The source of asymmetry between the S^x and S^z components of the spin is two-fold. One is due to the two-leg honeycomb strip connectivity, and the second is the finite tilting of the magnetic field which further enhances their difference. The preceding properties are shown for $N = 100, 200, 300, 400$, and iDMRG in Fig. 5 with different colors, and are seen to be relatively insensitive to the system size.

Underlying phase diagram. To understand the microscopic mechanism of the emerging KSL, we study the $K - \Gamma$ model without Γ' —i.e., in the absence of small interactions that induce ZZ order—at $\theta = 0$. At zero field, there is a finite region of the KSL when the AFM off-diagonal symmetric Γ interaction is

introduced. Then in zero field at Γ/K_c there is a transition from the KSL to another possible spin liquid dubbed KT spin liquid (KTSL)²⁸. Components of the spin–spin correlators, $\langle S^x S^x \rangle$ and $\langle S^z S^z \rangle$ shown in Fig. 6a, b, demonstrate a lack of magnetic order in the KSL and KTSL at $h = 0$, and finite correlations building with increasing field.

The KTSL is characterized by a finite $\langle W_p W_{p'} \rangle$ like the KSL, but with negative $\langle W_p \rangle$ as shown in Fig. 6c, d. While $\langle W_p \rangle$ is positive in the KSL, a negative $\langle W_p \rangle$ in the KTSL indicates a phase with a finite flux density. Strikingly, when the field is applied along the [111] direction the KSL sits above the KTSL for a fixed Γ/K , leading to two phase transitions with increasing field: KTSL \rightarrow KSL \rightarrow PS. The KTSL is extremely fragile to additional interactions that stabilize ZZ order. For example, when a small Γ' interaction is introduced the KTSL is replaced by the ZZ ordered phase as shown in Fig. 1. Importantly, the ZZ order does not extend all the way to the Kitaev limit and leaves a finite region of the KSL at zero field.

Discussion

Here we presented a microscopic theory, based on dominant Kitaev and off-diagonal symmetric Γ interactions, which offers an intermediate KSL emerging between the low-field and high-field states. The low-field ZZ state is induced via small perturbations beyond K and Γ , such as Γ' due to trigonal distortion of ligand octahedra. Our numerical data indicates that this additional interaction can wipe

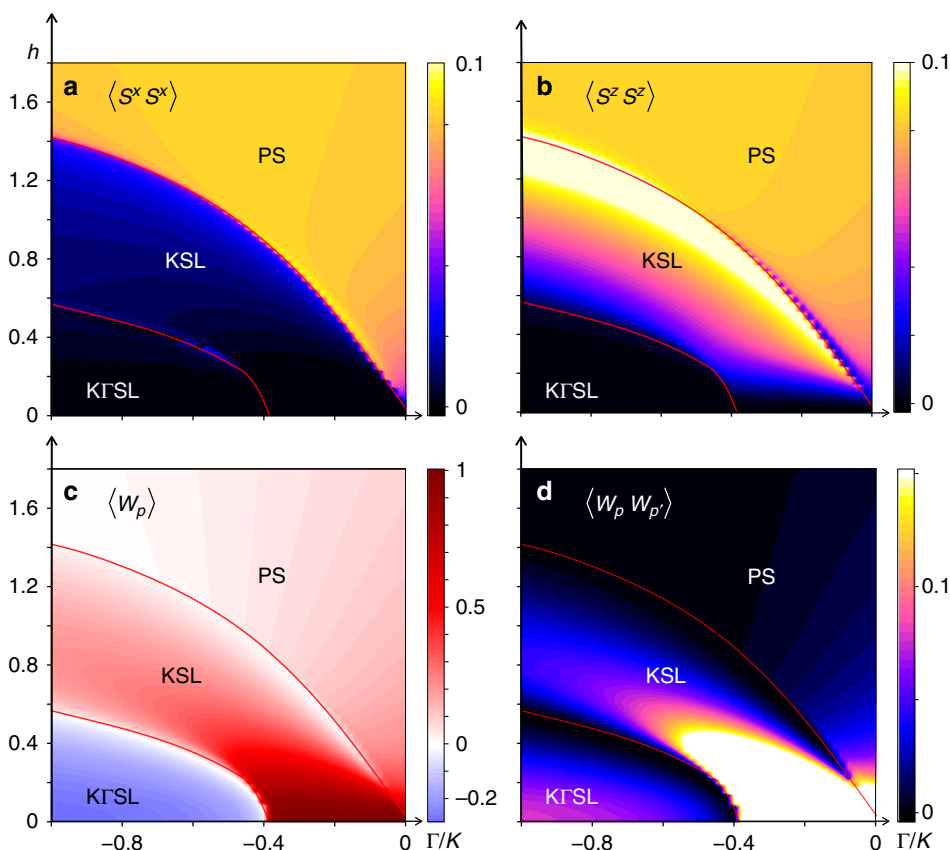


Fig. 6 Underlying phase diagram. Underlying phase diagram with $\Gamma' = 0$ and $\theta = 0$ in the $\Gamma/K - h$ plane as calculated with DRMG for $N = 200$ and OBC. Spin–spin correlations **a** $\langle S_j^x S_k^x \rangle$ and **b** $\langle S_j^z S_k^z \rangle$ at $k - j = 50$ are absent within the KTSL and the KSL phases at $h = 0$, and develop under the field. Phase boundaries, determined by smoothed fits to the peaks of χ_h and $\chi_{\Gamma/K}$, are drawn as red lines, and separate the KTSL and the PS from the intervening KSL. **c** Plaquette expectation $\langle W_p \rangle$ differentiates the KTSL and the KSL as it changes sign across the transition. **d** Plaquette–plaquette correlations $\langle W_p W_{p'} \rangle$ at $p' - p = 30$ are small in the PS and become appreciable within the KTSL and KSL, approaching $\langle W_p \rangle^2$ in the limit of large separation

out the KSL phase (including the pure Kitaev limit at $h = 0$) when its strength is too large, leading to a single transition between ZZ and PS under a magnetic field. Experimental reports of a half-quantized thermal Hall conductivity in α -RuCl₃ imply that the strengths of interactions beyond K and Γ are small enough to leave the intermediate KSL intact, yet finite to induce the ZZ order. In the absence of these interactions the K - Γ model exhibits another possible spin liquid called the KTSL, which is then replaced by the ZZ due to these small interactions. It is possible that a region of the KTSL survives with smaller Γ' while developing ZZ order, resulting in two spin liquids between ZZ and PS under a field. We leave these questions for a future study.

As the magnetic field is tilted away from the out-of-plane $[111]$ direction towards the in-plane $[11\bar{2}]$ direction the intermediate KSL region shrinks rapidly— independent of the strength of Γ' and for both cluster shapes studied here. What remains is a small intermediate phase at fields an order of magnitude smaller for moderate $\Gamma/|K|$, showing a dramatic magnetic anisotropy. Considering an anisotropic g -factor, due to a combination of the layered structure and SOC, the magnetic anisotropy is further enhanced by the ratio between the in-plane g_{ab} and the out-of-plane g_c components. While smaller tilting angles are less effective at destroying the ZZ magnetic order, they offer a much larger region of the KSL. To enlarge the intermediate KSL phase, we therefore propose that a field should be applied at smaller tilting angles. Further thermal Hall transport measurements for different in-plane components would be desirable in order to test our microscopic theory.

There are several aspects of this work that require further study. The first is the presence of large fluctuations in $\langle W_p W_{p'} \rangle$ and $\langle S_j^x S_k^x \rangle$ just above the KSL phase into the PS, which is also seen by $\chi_{\Gamma/K}$ and an unsaturated magnetization in the 24-site honeycomb cluster. This is suggestive of a non-trivial crossover region into the fully polarized phase. We also note the presence of a non-magnetic phase dubbed KTSL in the underlying phase diagram of the K - Γ model on the two-leg geometry next to the KSL phase. The KTSL at zero field is differentiated from the KSL by a sharp drop from $\langle W_p \rangle = 1$ in the KSL to $\langle W_p \rangle \simeq -\frac{1}{3}$ in the KTSL, accompanied by a singular $\chi_{\Gamma/K}$. Nature of the KTSL, numerical studies of this phase in the honeycomb geometry, and the transition to the KSL are excellent subjects for future study. For instance, studies of possible vortex patterns due to strong interactions among MFs and \mathbb{Z}_2 vortices would be highly interesting to pursue.

Methods

Details of simulations. Numerical exact diagonalization (ED), and density matrix renormalization group (DMRG) are used to study the parameter space appropriate for α -RuCl₃. In the ED and DMRG calculations, we consider the two-leg honeycomb strip geometry, and the 24-site honeycomb shape in ED only, both shown in Supplementary Fig. 1. The choice of these clusters is discussed in Supplementary Note 1, and is related to hidden points of SU(2) symmetry present in the 2D limit.

ED was performed on the 24-site honeycomb cluster with periodic boundary conditions, where the Lanczos method was used to obtain the lowest-lying eigenvalues and eigenvectors of the Hamiltonian in Eq. (1).

Part of the numerical calculations were performed using the ITensor library (<http://itensor.org>) typically with a target precision of 10^{-11} using up to 1000 states. All DMRG calculations were performed using open boundary conditions (OBC). The iDMRG calculations were performed using a target precision of 5×10^{-11} and up to 1000 states.

Data availability

The data that support the findings of this study are available from the corresponding author upon reasonable request.

Code availability

The code used to generate the data used in this study is available from the corresponding author upon reasonable request.

Received: 18 January 2019 Accepted: 9 May 2019

Published online: 06 June 2019

References

- Kitaev, A. Anyons in an exactly solved model and beyond. *Ann. Phys.* **321**, 2–111 (2006).
- Balents, L. Spin liquids in frustrated magnets. *Nature* **464**, 199 (2010).
- Zhou, Y., Kanoda, K. & Ng, T.-K. Quantum spin liquid states. *Rev. Mod. Phys.* **89**, 025003 (2017).
- Nayak, C., Simon, S. H., Stern, A., Freedman, M. & Sarma, S. D. Non-Abelian anyons and topological quantum computation. *Rev. Mod. Phys.* **80**, 1083–1159 (2008).
- Jackeli, G. & Khaliullin, G. Mott insulators in the strong spin-orbit coupling limit: from Heisenberg to a quantum compass and Kitaev models. *Phys. Rev. Lett.* **102**, 017205 (2009).
- Chaloupka, J., Jackeli, G. & Khaliullin, G. Kitaev-Heisenberg model on a honeycomb lattice: possible exotic phases in iridium oxides A₂IrO₃. *Phys. Rev. Lett.* **105**, 027204 (2010).
- Witczak-Krempa, W., Chen, G., Kim, Y. B. & Balents, L. Correlated quantum phenomena in the strong spin-orbit regime. *Annu. Rev. Condens. Matter Phys.* **5**, 57–82 (2014).
- Rau, J. G., Lee, E.-H. & Kee, H.-Y. Spin-orbit physics giving rise to novel phases in correlated systems: Iridates and related materials. *Annu. Rev. Condens. Matter Phys.* **7**, 195–221 (2016).
- Winter, S. M. et al. Models and materials for generalized Kitaev magnetism. *J. Phys. Condens. Matter* **29**, 493002 (2017).
- Singh, Y. et al. Relevance of the Heisenberg-Kitaev model for the honeycomb lattice iridates A₂IrO₃. *Phys. Rev. Lett.* **108**, 127203 (2012).
- Modic, K. A. et al. Realization of a three-dimensional spin-anisotropic harmonic honeycomb iridate. *Nat. Commun.* **5**, 4203 (2014).
- Rau, J. G., Lee, E.-H. & Kee, H.-Y. Generic spin model for the honeycomb iridates beyond the Kitaev limit. *Phys. Rev. Lett.* **112**, 077204 (2014).
- Rau, J. G. & Kee, H.-Y. Trigonal distortion in the honeycomb iridates: Proximity of zigzag and spiral phases in Na₂IrO₃. Preprint at <http://arXiv.org/abs/1408.4811> (2014).
- Plumb, K. W. et al. α -RuCl₃: A spin-orbit assisted Mott insulator on a honeycomb lattice. *Phys. Rev. B* **90**, 041112 (2014).
- Sandilands, L. J., Tian, Y., Plumb, K. W., Kim, Y.-J. & Burch, K. S. Scattering continuum and possible fractionalized excitations in α -RuCl₃. *Phys. Rev. Lett.* **114**, 147201 (2015).
- Kim, H.-S., Shankar, V. V., Catuneanu, A. & Kee, H.-Y. Kitaev magnetism in honeycomb α -RuCl₃ with intermediate spin-orbit coupling. *Phys. Rev. B* **91**, 241110 (2015).
- Banerjee, A. et al. Proximate Kitaev quantum spin liquid behaviour in a honeycomb magnet. *Nat. Mater.* **15**, 733 (2016).
- Sandilands, L. J. et al. Spin-orbit excitations and electronic structure of the putative Kitaev magnet α -RuCl₃. *Phys. Rev. B* **93**, 075144 (2016).
- Choi, S. K. et al. Spin waves and revised crystal structure of honeycomb iridate Na₂IrO₃. *Phys. Rev. Lett.* **108**, 127204 (2012).
- Chaloupka, J., Jackeli, G. & Khaliullin, G. Zigzag magnetic order in the iridium oxide Na₂IrO₃. *Phys. Rev. Lett.* **110**, 097204 (2013).
- Fletcher, J. M., Gardner, W. E., Fox, A. C. & Topping, G. X-ray, infrared, and magnetic studies of α - and β -ruthenium trichloride. *J. Chem. Soc. A*, 1038–1045 (1967).
- Sears, J. A. et al. Magnetic order in α -RuCl₃: A honeycomb-lattice quantum magnet with strong spin-orbit coupling. *Phys. Rev. B* **91**, 144420 (2015).
- Johnson, R. D. et al. Monoclinic crystal structure of α -RuCl₃ and the zigzag antiferromagnetic ground state. *Phys. Rev. B* **92**, 235119 (2015).
- Cao, H. B. et al. Low-temperature crystal and magnetic structure of α -RuCl₃. *Phys. Rev. B* **93**, 134423 (2016).
- Kim, H.-S. & Kee, H.-Y. Crystal structure and magnetism in α -RuCl₃: an ab initio study. *Phys. Rev. B* **93**, 155143 (2016).
- Janssen, L., Andrade, E. & Vojta, M. Magnetization processes of zigzag states on the honeycomb lattice: identifying spin models for α -RuCl₃ and Na₂IrO₃. *Phys. Rev. B* **96**, 064430 (2017).
- Yadav, R. et al. Kitaev exchange and field-induced quantum spin-liquid states in honeycomb α -RuCl₃. *Sci. Rep.* **6**, 37925 (2016).
- Lampen-Kelley, P. et al. Field-induced intermediate phase in α -RuCl₃: Non-coplanar order, phase diagram, and proximate spin liquid. Preprint at <http://arXiv.org/abs/1807.06192> (2018).
- Liu, Z.-X. & Normand, B. Dirac and chiral quantum spin liquids on the honeycomb lattice in a magnetic field. *Phys. Rev. Lett.* **120**, 187201 (2018).
- Baek, S.-H. et al. Evidence for a field-induced quantum spin liquid in α -RuCl₃. *Phys. Rev. Lett.* **119**, 037201 (2017).

31. Wolter, A. U. B. et al. Field-induced quantum criticality in the Kitaev system α -RuCl₃. *Phys. Rev. B* **96**, 041405 (2017).
32. Zheng, J. et al. Gapless spin excitations in the field-induced quantum spin liquid phase of α -RuCl₃. *Phys. Rev. Lett.* **119**, 227208 (2017).
33. Janša, N. et al. Observation of two types of fractional excitation in the Kitaev honeycomb magnet. *Nat. Phys.* **14**, 786–790 (2018).
34. Kasahara, Y. et al. Majorana quantization and half-integer thermal quantum Hall effect in a Kitaev spin liquid. *Nature* **559**, 227–231 (2018).
35. Vinkler-Aviv, Y. & Rosch, A. Approximately quantized thermal Hall effect of chiral liquids coupled to phonons. *Phys. Rev. X* **8**, 031032 (2018).
36. Cookmeyer, J. & Moore, J. E. Spin-wave analysis of the low-temperature thermal Hall effect in the candidate Kitaev spin liquid α -RuCl₃. *Phys. Rev. B* **98**, 060412 (2018).
37. Ye, M., Halász, G. B., Savary, L. & Balents, L. Quantization of the thermal Hall conductivity at small Hall angles. *Phys. Rev. Lett.* **121**, 147201 (2018).
38. Jiang, H.-C., Gu, Z.-C., Qi, X.-L. & Trebst, S. Possible proximity of the Mott insulating iridate Na₂IrO₃ to a topological phase: phase diagram of the Heisenberg-Kitaev model in a magnetic field. *Phys. Rev. B* **83**, 245104 (2011).
39. Zhu, Z., Kimchi, I., Sheng, D. N. & Fu, L. Robust non-Abelian spin liquid and a possible intermediate phase in the antiferromagnetic Kitaev model with magnetic field. *Phys. Rev. B* **97**, 241110 (2018).
40. Liang, S., Jiang, M.-H., Chen, W., Li, J.-X. & Wang, Q.-H. Intermediate gapless phase and topological phase transition of the Kitaev model in a uniform magnetic field. *Phys. Rev. B* **98**, 054433 (2018).
41. Gohlke, M., Moessner, R. & Pollmann, F. Dynamical and topological properties of the Kitaev model in a [111] magnetic field. *Phys. Rev. B* **98**, 014418 (2018).
42. Nasu, J., Kato, Y., Kamiya, Y. & Motome, Y. Successive Majorana topological transitions driven by a magnetic field in the Kitaev model. *Phys. Rev. B* **98**, 060416 (2018).
43. Hickey, C. & Trebst, S. Emergence of a field-driven U(1) spin liquid in the Kitaev honeycomb model. *Nat. Commun.* **10**, 530 (2019).
44. Ronquillo, D. C., Vengal, A. & Trivedi, N. Field-orientation-dependent spin dynamics of the Kitaev honeycomb model. Preprint at <http://arXiv.org/abs/1805.03722> (2018).
45. Jiang, H.-C., Wang, C.-Y., Huang, B. & Lu, Y.-M. Field induced quantum spin liquid with spinon Fermi surfaces in the Kitaev model. Preprint at <http://arXiv.org/abs/1809.08247> (2018).
46. Zou, L. & He, Y.-C. Field-induced neutral Fermi surface and QCD₃-Chern-Simons quantum criticalities in Kitaev materials. Preprint at <http://arXiv.org/abs/1809.09091> (2018).
47. Patel, N.-D. & Trivedi, N. Magnetic field induced intermediate quantum spin-liquid with a spinon Fermi surface. Preprint at <http://arXiv.org/abs/1812.06105> (2018).
48. Catuneanu, A., Yamaji, Y., Wachtel, G., Kim, Y. B. & Kee, H.-Y. Path to stable quantum spin liquids in spin-orbit coupled correlated materials. *npj Quantum Mater.* **3**, 23 (2018).
49. Gohlke, M., Wachtel, G., Yamaji, Y., Pollmann, F. & Kim, Y. B. Quantum spin liquid signatures in Kitaev-like frustrated magnets. *Phys. Rev. B* **97**, 075126 (2018).
50. Banerjee, A. et al. Excitations in the field-induced quantum spin liquid state of α -RuCl₃. *npj Quantum Mater.* **3**, 8 (2018).
51. Winter, S. M., Li, Y., Jeschke, H. O. & Valentí, R. Challenges in design of Kitaev materials: Magnetic interactions from competing energy scales. *Phys. Rev. B* **93**, 214431 (2016).
52. Catuneanu, A., Sørensen, E.-S. & Kee, H.-Y. Non-local string order parameter in the $s = 1/2$ Kitaev-Heisenberg ladder. *Phys. Rev. B* **99**, 195112 (2019).

Acknowledgements

This work was supported by the Natural Sciences and Engineering Research Council of Canada and the Center for Quantum Materials at the University of Toronto. This research was enabled in part by support provided by Sharcnet (<http://www.sharcnet.ca>) and Compute Canada (<http://www.computecanada.ca>). Computations were performed on the GPC and Niagara supercomputers at the SciNet HPC Consortium. SciNet is funded by: the Canada Foundation for Innovation under the auspices of Compute Canada; the Government of Ontario; Ontario Research Fund—Research Excellence; and the University of Toronto.

Author contributions

Exact diagonalization calculations were performed by J.S.G. and A.C. Density-matrix renormalization group calculations were performed by E.S.S. H.-Y.K. planned and supervised the project. All authors wrote the manuscript.

Additional information

Supplementary Information accompanies this paper at <https://doi.org/10.1038/s41467-019-10405-8>.

Competing interests: The authors declare no competing interests.

Reprints and permission information is available online at <http://npg.nature.com/reprintsandpermissions/>

Journal peer review information: *Nature Communications* thanks the anonymous reviewers for their contribution to the peer review of this work.

Publisher's note: Springer Nature remains neutral with regard to jurisdictional claims in published maps and institutional affiliations.



Open Access This article is licensed under a Creative Commons Attribution 4.0 International License, which permits use, sharing, adaptation, distribution and reproduction in any medium or format, as long as you give appropriate credit to the original author(s) and the source, provide a link to the Creative Commons license, and indicate if changes were made. The images or other third party material in this article are included in the article's Creative Commons license, unless indicated otherwise in a credit line to the material. If material is not included in the article's Creative Commons license and your intended use is not permitted by statutory regulation or exceeds the permitted use, you will need to obtain permission directly from the copyright holder. To view a copy of this license, visit <http://creativecommons.org/licenses/by/4.0/>.

© The Author(s) 2019